Received: 12 May 2022 | Revised: 13 September 2023 | Accepted: 21 September 2023

DOI: 10.1096/fj.202200692RRRR

RESEARCH ARTICLE

The FASEB Journal

ADAMTS12 is a stromal modulator in chronic liver disease

Bassil Dekky[1] | **Fida Azar**[1] | **Dominique Bonnier**[1] | **Christine Monseur**[2] | **Chiara Kalebić**[1] | **Esther Arpigny**[2] | **Alain Colige**[2] | **Vincent Legagneux**[1] | **Nathalie Théret**[1]

[1]University of Rennes, INSERM, EHESP, IRSET (Institut de Recherche en Santé, Environnement et Travail)—UMR_S 1085, Rennes, France

[2]Laboratory of Connective Tissues Biology, GIGA-R, University of Liege, Liege, Belgium

Correspondence
Nathalie Théret, INSERM U1085-IRSET, 2 Av Pr. Léon Bernard, 35043 Rennes, France.
Email: nathalie.theret@inserm.fr

Present address
Bassil Dekky, PIC Therapeutics, Natick, Massachusetts, USA

Fida Azar, Unité de Nutrition Humaine, INRAE, Université Clermont Auvergne, UMR1019, Clermont-Ferrand, France

Chiara Kalebić, Molecular Virology Laboratory, International Centre for Genetic Engineering and Biotechnology (ICGEB), Trieste, Italy

Funding information
Fonds De La Recherche Scientifique - FNRS (FNRS), Grant/Award Number: 7.6536.18; Ligue Contre le Cancer (French League Against Cancer)

Abstract

Adamalysins, a family of metalloproteinases containing a disintegrin and metalloproteinases (ADAMs) and ADAM with thrombospondin motifs (ADAMTSs), belong to the matrisome and play important roles in various biological and pathological processes, such as development, immunity and cancer. Using a liver cancer dataset from the International Cancer Genome Consortium, we developed an extensive in silico screening that identified a cluster of adamalysins co-expressed in livers from patients with hepatocellular carcinoma (HCC). Within this cluster, *ADAMTS12* expression was highly associated with recurrence risk and poorly differentiated HCC signatures. We showed that *ADAMTS12* was expressed in the stromal cells of the tumor and adjacent fibrotic tissues of HCC patients, and more specifically in activated stellate cells. Using a mouse model of carbon tetrachloride-induced liver injury, we showed that A*damts12* was strongly and transiently expressed after a 24 h acute treatment, and that fibrosis was exacerbated in *Adamts12*-null mice submitted to carbon tetrachloride-induced chronic liver injury. Using the HSC-derived LX-2 cell line, we showed that silencing of *ADAMTS12* resulted in profound changes of the gene expression program. In particular, genes previously reported to be induced upon HSC activation, such as PAI-1, were mostly down-regulated following *ADAMTS12* knock-down. The phenotype of these cells was changed to a less differentiated state, showing an altered actin network and decreased nuclear spreading. These phenotypic changes, together with the down-regulation of PAI-1, were offset by TGF-β treatment. The present study thus identifies ADAMTS12 as a modulator of HSC differentiation, and a new player in chronic liver disease.

Abbreviations: ADAM, a disintegrin and metalloprotease; ADAMTS, ADAM with thrombospondin type I motifs; COL1A1, alpha-1 type-1 collagen; CTGF, connective tissue growth factor; ECM, extracellular matrix; CCl_4, carbon tetrachloride; HCC, hepatocellular carcinoma; HSC, hepatic stellate cell; MMP2, matrix metalloproteinase 2; MMP9, matrix metalloproteinase 9; MSC, mesenchymal stem cell; PAI1, plasminogen activator inhibitor 1; TCGA, The Cancer Genome Atlas Program; TGF-β, transforming growth factor-beta.

Bassil Dekkya and Fida Azar contributed equally to this work.

KEYWORDS
adamalysins, ADAMTS12, hepatocellular carcinoma, liver fibrosis

1 | INTRODUCTION

Most chronic liver diseases are associated with a progressive fibrosis characterized by excessive accumulation of extracellular matrix (ECM) that impairs liver functions. With end-stage cirrhosis, there is an increasing risk of complications, including ascites, variceal bleeding and cancer. Cirrhosis is the main cause of hepatocellular carcinoma (HCC), and we previously demonstrated that ECM remodeling in adjacent fibrotic liver is associated with tumor progression in patients with HCC.[1] ECM remodeling refers to the dynamics of synthesis and degradation of matrix components that occurs during both liver regeneration and fibrosis.[2] Consistently, dynamic changes of the matrisome, which encompasses ECM and ECM-associated proteins,[3] have been observed in response to liver injury.[4] By producing matrix macromolecules and secreting matrix metalloproteases (MMPs) and tissue inhibitors of MMPs (TIMPs), activated hepatic stellate cells (HSCs) are the main drivers of ECM and tissue remodeling in response to liver injury.[5] Consistently, dynamic changes of the matrisome, which encompasses ECM and ECM-associated proteins,[3] have been observed in response to liver injury.[4] While MMPs have been widely implicated in ECM remodeling, metalloproteinases from the adamalysin family have been more recently associated with liver fibrosis and hepatocellular carcinoma progression (reviewed in Ref. [6]). Adamalysins constitute a family of proteins containing a disintegrin and metalloproteinases (ADAMs)[7] and ADAM with thrombospondin motifs (ADAMTSs),[8] which have been classified as ECM regulators of the matrisome (http://matrisomeproject.mit.edu). More specifically, ADAMs are mainly transmembrane proteins that have been implicated in cell adhesion, migration, signaling and juxtamembrane proteolysis (sheddase activity) while ADAMTS are secreted proteins that bind to ECM and are involved in collagen processing, matrix degradation and activation of growth factors. These proteins are therefore likely to be involved in the regulation of tissue repair and fibrosis. However, the role of most of the 21 ADAMs and 19 ADAMTSs in pathophysiology remains unclear. We previously showed that overexpression of ADAM12 in activated HSCs is associated with tumor aggressiveness[9] and that ADAM12 interacts with the TGF-β receptor TGFBR2[10] and with ILK[11] to promote Smad- and non-Smad-dependent TGF-β signaling pathways. Activated HSCs are also a source of ADAM9,[9,12,13] ADAM8 and 28,[13] ADAM10,[14] and ADAM17.[14–17] Some of these ADAMs contribute to tumor cell invasion[12] and epidermal growth factor receptor transactivation.[16] Accordingly, up-regulation of these ADAMs has been reported in hepatocellular carcinoma[18] and targeting ADAM10 has been recently proposed for reduction of tumor invasion.[19] Relatively few ADAMTSs have been implicated in chronic liver disease. ADAMTS1 has been cloned from cirrhotic liver samples[20] and was demonstrated to activate TGF-β in HSCs during liver fibrosis.[21] The procollagen-N-proteinase ADAMTS2 that is implicated in the maturation of collagen is a critical regulator of fibrosis since its silencing attenuates CCl_4-induced fibrosis.[22] More recently, ADAMTS2 was shown to be involved in the control of TGF-β activity in human fibroblasts.[23] Similarly, ADAMTS5 deficiency protects against non-alcoholic steatohepatitis in obesity through a decrease of proteolytic remodeling of the ECM.[24] By contrast, ADAMTS7 knock-out mice showed increased biliary fibrosis associated with an increase of its substrate Connective Tissue Growth Factor (CTGF).[25] ADAMTS13, which cleaves von Willebrand factor (vWF), is produced by HSCs. Deficiency or alteration of ADAMTS13 leads to accumulation of unusually large vWF multimers, contributing to liver injuries.[26] In order to explore the roles of the entire family of adamalysins in chronic liver diseases, we developed a large in silico screening for adamalysin expression in tissue samples from patients with HCC, using RNAseq data from the TCGA LIHC-US database. This enabled us to show that *ADAMTS12* expression is linked to chronic liver disease and HCC progression, and to demonstrate its role in the response to liver injury and in HSC differentiation.

2 | MATERIALS AND METHODS

2.1 | Human tissue samples

Tumor and matching non-tumor liver samples were obtained from patients undergoing surgical hepatectomy as previously described.[1] Histological stages of fibrosis were graded according to the METAVIR score: F1, portal fibrosis without septa; F2, portal fibrosis with rare septa; F3, numerous septa without cirrhosis; and F4, cirrhosis. Inflammatory activity was graduated as A0, no activity; A1, mild activity; and A2, moderate activity. All tissue sections were routinely analyzed after staining with hematoxylin–eosin-saffron and Sirius red. Liver samples were from the Biological Resources Center (BRC) at Rennes University

Hospital. Access to this material was in agreement with French laws and satisfied the requirements of the local Ethics Committee.

2.2 | In-situ hybridization and immunodetection on tissue sections

Tissue samples were formalin fixed and paraffin embedded (FFPE). 5 µm tissue sections were deparaffinized with xylene (2 × 5 min), rehydrated with decreasing concentrations of ethanol (100%–60%–30% for 2 min each), washed with distilled water and then dried for 10 min at room temperature. Detection and localization of mRNAs in tissue samples was performed using the RNAscope® in-situ hybridization (ISH) assay according to the manufacturer's instructions (Advanced Cell Diagnostics Inc., HAYWARD, CA, USA). For single ISH labeling, we used RNAscope® 2.5 HD Reagent Kit-RED (Fast-Red labeling) with the human *ADAMTS12* probe predesigned by the manufacturer: RNAscope® Probe-Hs-ADAMTS12 (Cat No. 507691). The negative control probe used was Probe-DapB (Cat No. 31043). For double ISH labeling we used RNAscope™ 2.5 HD Duplex Assay (Cat No. 322435) with ADAMTS12 (Cat No. 507691-C2) and ACTA2 (Cat No. 444771) probes. ISH signals were detected with Fast-Red (*ADAMTS12* probe, red) and HRP (ACTA2 probe, green). After mRNA detection, slides were either counter-stained in 25% Hematoxylin or stored in PBS for immunostaining. Immunodetection was performed after ISH detection and on the same sections, except for CD45 and CD34 antigens whose detection was not compatible with sample treatments required for ISH. For these two antigens, ISH and immunodetection were therefore performed on two adjacent 5 µm sections. Antibodies were used in PBS containing 1% BSA. Antibodies and dilutions were as follows: alpha-SMA (Dako M0851, 1:200), Collagen 1 (Sigma Ab758, 1:100), CD14 (AbCam ab183322, 1:1000), CD45 (Dako M0701, 1:100), CD68 (Dako M0876, 1:100), CD34 (Invitrogen MA5-32059, 1:500), GFAP (Dako Z0334, 1:200), GPR91/SUCNR1 (LSBio LS-B6591-50, 1/200). Pictures were acquired using a slide NanoZoomer scanner (Hamamatsu C10730-12) using the NDP.scan 3.4.0 software. Scoring positive cells for a given marker was performed using QuPath: Vessels were delineated using the "magic wand" tool, annotated as vessels and substracted (tissueGeom. difference script command) from the entire section picture. Cells were detected using the "Cell detection" tool with default parameters and a cell expansion of 10 μm^2 (detection of GFAP-positive cells) or 1 μm^2 (detetion of GPR91-positive cells). Measurements were recorded into a single table and analyzed with R.

2.3 | Animal models and CCl_4 administration

Adamts12$^{-/-}$ mice were generated and genotyped as previously described.[27] For all treatments, eight-week-old females were treated by intraperitoneal injections of CCl_4 (Sigma-Aldrich, St. Louis, MO, USA) diluted at 3% v/v in olive oil. Control mice were treated with the vehicle (olive oil). For chronic treatment, doses of 0.3 mL/kg of mouse body weight were administered 3 times per week for 4 weeks. Mice were sacrificed 4 days (peak of fibrosis) or 18 days (2 weeks of recovery) after the last injection of CCl_4. For acute treatment, a single dose of 0.3 mL/kg of mouse body weight was administered and mice were sacrificed after 4, 12, 24 h or 7 days. Livers were collected, weighed and treated as previously described.[22] All experiments were carried out following the guidelines of the Committee on Animal Experimentation of the University of Liege, Belgium.

2.4 | Blood enzyme analyses

Blood was collected by cardiac puncture and centrifuged at 2500 rpm for 25 min at 4°C, and plasma (supernatant) was collected and diluted four-fold with PBS. The activity of alanine aminotransferase (ALT) in the plasma was measured according to the IFCC primary reference procedures using an Olympus AU2700 Autoanalyzer (Olympus Optical, Tokyo, Japan).

2.5 | RNA isolation and quantitative real-time PCR

Liver samples were collected in RNAlater®, and total RNA was extracted using TRIzol (Invitrogen) reagent according to the manufacturer's instructions. Reverse transcription was performed using Superscript II (Invitrogen). Real-time quantitative PCR was performed with Power-SYBR-Green PCR Master Mix (Applied Biosystems). Transcript abundance was normalized using the GAPDH reference gene. Primer sequences are provided in Table S1.

2.6 | Cell culture and cytological analysis

LX-2 and MRC-5 cell lines were cultured in DMEM containing 4.5 g/L Glucose, Pyruvate, Glutamine, penicillin (100 IU/mL)-streptomycin (100 mg/mL) and supplemented with 10% fetal calf serum (Eurobio). Primary human hepatocytes and HSCs were isolated from

histologically normal specimens from patients undergoing hepatic resection for liver metastases, as previously described.[9] HSCs and freshly isolated human hepatocytes were cultured in DMEM containing 4.5 g/L glucose, pyruvate, glutamine, penicillin (100 IU/mL)-streptomycin (100 mg/mL) and supplemented with 2 mM glutamine and 10% fetal calf serum (Lonza). When indicated, cells were treated with 3 ng/mL of IL1-β or 5 ng/mL TGF-β. For TGF-β treatment, cells were cultured for 15 h in media containing 2% fetal calf serum prior to TGF-β (5 ng/mL) addition for the indicated times.

For immunodetection, cells were fixed for 10 min in 4% paraformaldehyde, permeabilized with 0.1% Triton X-100 in PBS, and washed three times in PBS. For immunostaining, slides were incubated for 1 h at room temperature in PBS containing 1% BSA, then for 15 h at 4°C with primary antibodies, rinsed in PBS and incubated 1 h at room temperature with secondary antibodies. Antibodies were used in PBS containing 1% BSA. The ARL13B antibody (Antibodies Inc. 73–287) was used at 1:200 dilution.

For F-Actin staining, cells were incubated with phalloidin coupled with Alexa-488 (Ozyme, catalog number 8878s) diluted 1/20 in PBS for 20 min.

Slides were washed in PBS, counterstained with Hoechst-33342 and observed under epifluorescence microscopy. Images were analyzed with ImageJ software. For nuclear size analysis, regions of interest (ROIs) corresponding to the projected areas of nuclei (Hoechst signal) were defined by automatic thresholding. For each ROI and channel, area, average signal value and integrated signal value were collected. Analyses of measurement tables were performed in R.

2.7 | Gelatinase assays

The enzymatic activities of MMP2 and MMP9 in cell supernatants were determined by gelatin zymography as previously described.[1]

2.8 | Gene silencing by RNA-interference

LX-2 cells were transfected with *ADAMTS12* or control siRNAs for 24 to 48 h using Lipofectamine® RNAiMAX Reagent according to the manufacturer's instructions. Small interfering RNAs were provided by Eurogentec:

si*ADAMTS12* sequence (sense): GCCAAAGUUUG GAGGGAAAdTdT.
siCTRL (negative control): Eurogentec reference SR-CL000-005.

2.9 | RNA-sequencing

RNA samples from siRNA-transfected or control LX-2 cells and from mouse liver samples (see above) were quality controlled by RNA integrity number (RIN) measurement on a Bioanalyzer with RNA 6000 Nano assays (Agilent). RINs were comprised between 9.2 and 9.9. RNA-sequencing libraries were prepared and quality-controlled (fragment sizes of approximately 260 bp) by the GenoBiRD facility (Nantes, France) using the TruSeq® Stranded mRNA Library Prep (96 samples) from Illumina. Multiplexed libraries were sequenced on a NovaSeq 6000. FASTQ reads were aligned on the reference genome (GRCh38) using the STAR software and read counts per genes were computed using htseq-count. Differential analyses were performed using the R-package DESeq2.

2.10 | Databases and bioinformatic tools

Expression data (normalized expression values) were extracted from the The Cancer Genome Atlas Program (TCGA) via the 'International Cancer Genome Consortium" (https://icgc.org/). 294 samples corresponding to HCC primary tumors were extracted from the TCGA LIHC-US project database.

To assess links between gene expression and HCC annotations, normalized expression values were merged with annotations of the corresponding samples from the Cancer Genome Atlas Network.[28] For quantitative annotations, a Pearson's correlation test was performed between expression values and annotation values. For qualitative annotations, the distribution of expression values between groups was assessed by a non-parametric Kruskal–Wallis test. *p*-Values were calculated and plotted as −Log10 (*p*-values) on heat maps. For a given annotation and a given gene, the smaller the *p*-value, the more predictive the gene expression values for this annotation. Functional annotation of genes was performed using WEB-based GEneSeTAnaLysisToolkit (http://www.webgestalt.org/option.php).

Expression levels of adamalysin genes in Liver Cancer Cell Lines were extracted from the Cancer Cell Line Encycopedia (CCLE) dataset: https://data.broadinstitute.org/ccle_legacy_data/mRNA_expression/CCLE_Expression_Entrez_2012-09-29.gct

Only cell lines whose names contained the string "_LIVER" where retained.

2.11 | Statistical analyses

Graphs and statistical analyses were done using R. Statistical differences between groups were assessed by

non-parametric Mann–Whitney (two groups) or Kruskal–Wallis (more than two groups) tests. In that case, comparisons between two groups used a *p*-value adjusted for multiple tests (Dunn test). Levels of significance are as follows: $*p < .05$, $**p < .01$ and $***p < .001$.

3 | RESULTS

3.1 | Identification of a cluster of co-regulated adamalysin genes in HCC

Using the Cancer Genome Atlas (TCGA) LIHC-US dataset,[28] we investigated the gene expression of adamalysins in 294 liver tumor samples from patients with HCC (primary tumors). Expression levels of 36 adamalysin genes (14 ADAMs, 16 ADAMTS and 6 ADAMTSL) were highly heterogeneous among HCC samples and their analysis did not identify clusters of HCCs sharing a specific signature of adamalysin expression profiles (Figure S1). To further characterize the expression of adamalysins in HCCs, we built a correlation matrix by calculating the correlation of gene expression levels for each pair of the 36 adamalysins expressed in the tumors (Table S2). A heat-map of this correlation matrix shows that adamalysin gene expression levels are strongly correlated in HCC samples, with a large majority of positive correlations (Figure 1A, pink to red hits). Expression of a limited number of adamalysins, including *ADAMTSL4* and *ADAMTS17*, is anti-correlated with that of other adamalysins (Figure 1A, blue hits). Hierarchical clustering of this correlation map identified a large cluster (Figure 1A, label "1") of 23 adamalysins with the highest correlation of expression in HCCs. Within this cluster, *ADAM10* and its close relative *ADAM17* had the highest correlation coefficient ($r = .85$). Another sub-cluster containing seven highly correlated adamalysins was identified (Figure 1A, label "2"). Interestingly this cluster includes *ADAMTS1* and *ADAMTS2*, two adamalysins previously associated with chronic liver disease,[21,22,29] *ADAMTS7* whose product cleaves CTGF (a pivotal factor in liver fibrosis),[25] and *ADAMTS4* and *ADAMTS15* whose product, like ADAMTS1, cleave versican and have been proposed as modulators of liver fibrosis.[30] This cluster also contains *ADAMTS12* whose role in chronic liver diseases has not yet been addressed to our knowledge.

3.2 | *ADAMTS12* expression is linked to recurrence risk and poorly differentiated HCC

To identify pathophysiological contexts that may explain the strong correlations in expression levels within this cluster of 7 adamalysins, we explored the database constructed by the Cancer Genome Atlas Research Network.[28] In this database, TCGA HCC samples are classified according to molecular and clinical features that are expressed as qualitative or quantitative variables. For a qualitative variable (classified into two or more groups), we compared the expression values of a given gene in these groups, whereas for a quantitative variable, we calculated the correlation between this variable and the gene expression values. The resulting *p*-values are shown in Table S3, and a heat map of these *p*-values is shown in Figure S2A. The clinical and molecular features for which the expression levels of the genes in the adamalysin cluster are most strongly associated are shown in Figure 1B. Within this cluster, *ADAMTS12* is the gene whose expression is most strongly associated (white/yellow hits corresponding to the lowest *p*-values) with annotations related to proliferation (NCIPHS), tumor progression (repressed Hippo signaling), recurrence rate (SNUR, RS65, RS65 score) and low differentiation states (NCIHS, CC-like, IDH_P). Examples of associations between *ADAMTS12* expression and SNUR recurrence signature (qualitative variable) and RS65 recurrence score (quantitative variable) are shown in Figure S2B,C, respectively. Together, these observations show that *ADAMTS12* expression is strongly associated with molecular signatures related to HCC progression and aggressiveness.

3.3 | *ADAMTS12* is expressed in both tumors and underlying fibrotic tissues from patients with HCC

We then compared *ADAMTS12* expression levels in tumors and adjacent non-tumor tissues, taking advantage of the availability of 45 matched tumor/non-tumor samples in the TCGA database (LIHC-US). As shown in Figure 2, *ADAMTS12* expression is highly variable in HCC samples, being either higher or lower in tumor samples compared to adjacent tissues.

Using a local cohort of 48 HCC patients, we confirmed that *ADAMTS12* is expressed in both tumor and non-tumor samples (Figure S3A). Because the underlying liver tissue in patients with HCC is mainly fibrotic, we used the same cohort to explore the association of *ADAMTS12* expression with fibrosis stages. Although *ADAMTS12* mRNA levels were not significantly related to individual fibrosis stages, *ADAMTS12* expression was higher in samples from pooled stages F3 or F4 compared to samples with either no (F0) or moderate (F1 or F2) fibrosis (Figure S3B).

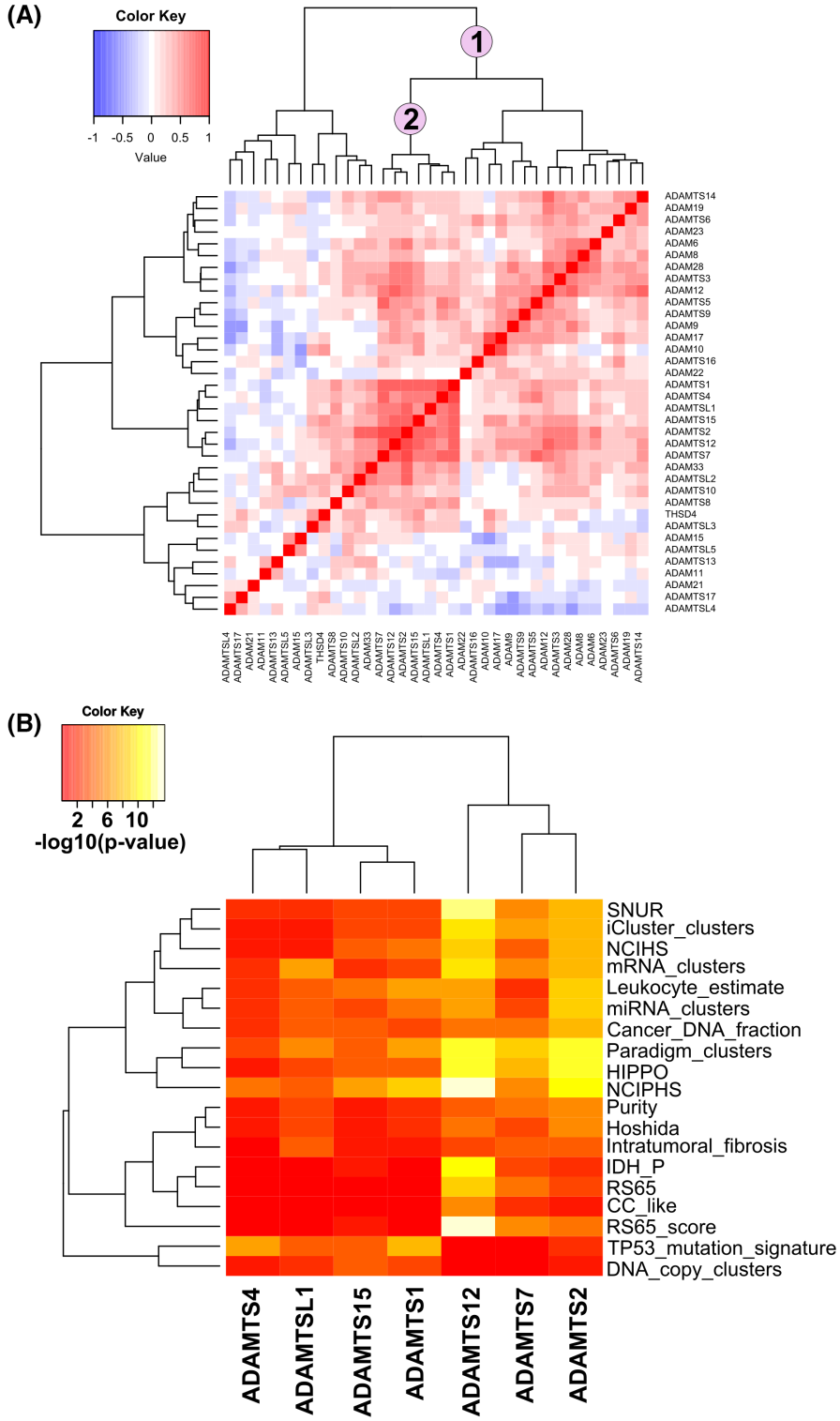

3.4 | Stromal cells are the main sources of ADAMTS12

To characterize the tissue structures in which *ADAMTS12* is expressed, we investigated the localization of *ADAMTS12* mRNAs in tumor samples, using in-situ hybridization. As shown in Figure 3A, *ADAMTS12* signal was restricted to a sub-population of cells with small, dense nuclei on hematoxylin-stained sample sections. These cells were clearly distinguishable from HCC cancer cells characterized by large, round-shaped nuclei. When quantifying *ADAMTS12* mRNAs in samples from five different HCC patients, we observed that *ADAMTS12* expression is highly heterogenous among and within samples (Figure S4A). Double-labeling experiments using probes against *ADAMTS12* and *ACTA2*

FIGURE 1 Identification of clusters of co-regulated adamalysins in liver samples from HCC patients. (A) Correlation map of adamalysin gene expression in HCC. Normalized gene expression values were extracted from the TCGA LIHC-US dataset. 294 HCC (LIHC-US data set) primary tumors were analyzed. Expression correlations (Pearson's coefficients) were calculated pair by pair for 36 adamalysin genes (ADAM, ADAMTS & ADAMTSL) expressed in these samples. The resulting correlation matrix (shown in Table S2) is presented as a heat map and used to identify clusters of co-regulated genes. A cluster of 23 correlated genes is labeled "1". This cluster contains a sub-cluster (labeled "2") of 7 genes whose expression levels are strongly correlated. The Pearson's correlation coefficients are represented by a color code from blue ($r=-1$) to red ($r=+1$). (B) Association between gene expression of adamalysins in cluster 2 and HCC annotations. Details and sources of the annotations are indicated in the Table S3. For a given gene, normalized expression values were extracted from each primary tumor samples (TCGA LIHC-US) and merged with annotations (Table S3) of the corresponding sample from the Cancer Genome Atlas Research Network.[28] The heat map represents *p*-values resulting from association tests for the most predictive variables. For a given annotation and a given gene, the smaller the *p*-value, the stronger the association (yellow-white hits) between gene expression values and annotation values in HCC samples. The complete heat map and calculation details are given in Figure S2, and correlation or non-parametric test *p*-values are provided in Table S3.

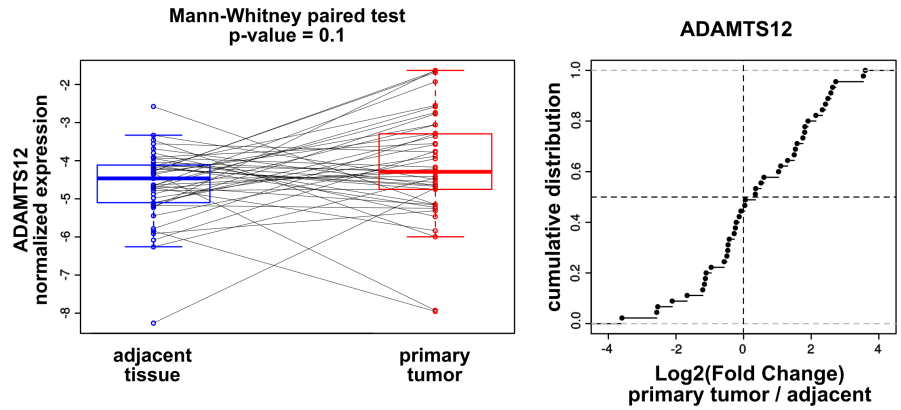

FIGURE 2 *ADAMTS12* expression in tumor and non-tumor tissues from patients with primary HCC. *ADAMTS12* mRNA levels were evaluated in paired tumor and adjacent non-tumor samples from the TCGA LIHC-US database (48 samples). Results are presented as paired expression values (left panel) or as a cumulative distribution of log-transformed fold changes between expression values in tumor and adjacent tissues (right panel).

(encoding α-SMA, a myofibroblast marker) mRNAs showed that cells expressing these genes were located in close proximity to each other. These regions contain cells that express either one of these mRNAs or both (Figure 3B), indicating that cells exhibiting a strong expression of ACTA2 are not the unique source of *ADAMTS12* expression. Consistently, the levels of correlation between *ADAMTS12* and *ACTA2* mRNA signals were highly heterogenous between and within patient biopsies (Figure S4B). By combining *ADAMTS12* mRNA detection by in-situ hybridization with α-SMA immunodetection, we confirmed that the density of *ADAMTS12*-expressing cells was higher in regions enriched in α-SMA-positive cells, with a limited number of cells expressing both markers (Figure 3C). These regions were also enriched in type I collagen (Figure 3D). To better characterize the microenvironment of *ADAMTS12* positive cells, we localized these cells with respect to monocytes ($CD14^+$), leukocytes ($CD45^+$) and endothelial cells ($CD34^+$) (Figure S5). This showed that *ADAMTS12* positive cells are distinct from monocytes and leukocytes, and we found only a limited number of endothelial cells ($CD34^+$) that expressed *ADAMTS12*.

In fibrotic tissues adjacent to tumors, similarly to the tumor tissues, *ADAMTS12* was expressed in cells with dense nuclei clearly distinguishable from hepatocytes (Figures 4A and S6A for higher resolution pictures). These *ADAMTS12*-expressing cells were in close proximity to cell clusters positive for α-SMA (Figure 4B), CD14 (Figure 4C) or CD68 (Figure 4D), markers of fibrosis, immune infiltrates, and resident macrophages (or Kupffer cells), respectively. These regions contained a limited number of cells positive for both α-SMA and *ADAMTS12*. In contrast, although located in very close proximity to immune infiltrates, *ADAMTS12*-positive cells were clearly distinct from monocytes (Figure 4C) and resident macrophages (Figure 4D).

When measured in isolated liver cells, *ADAMTS12* expression was significantly higher in cultured HSCs and the derived cell line LX-2 compared with resident macrophages (or Kupffer's cells), primary hepatocytes, or the HCC cell line Huh7 (Figure S6A). Consistent with these

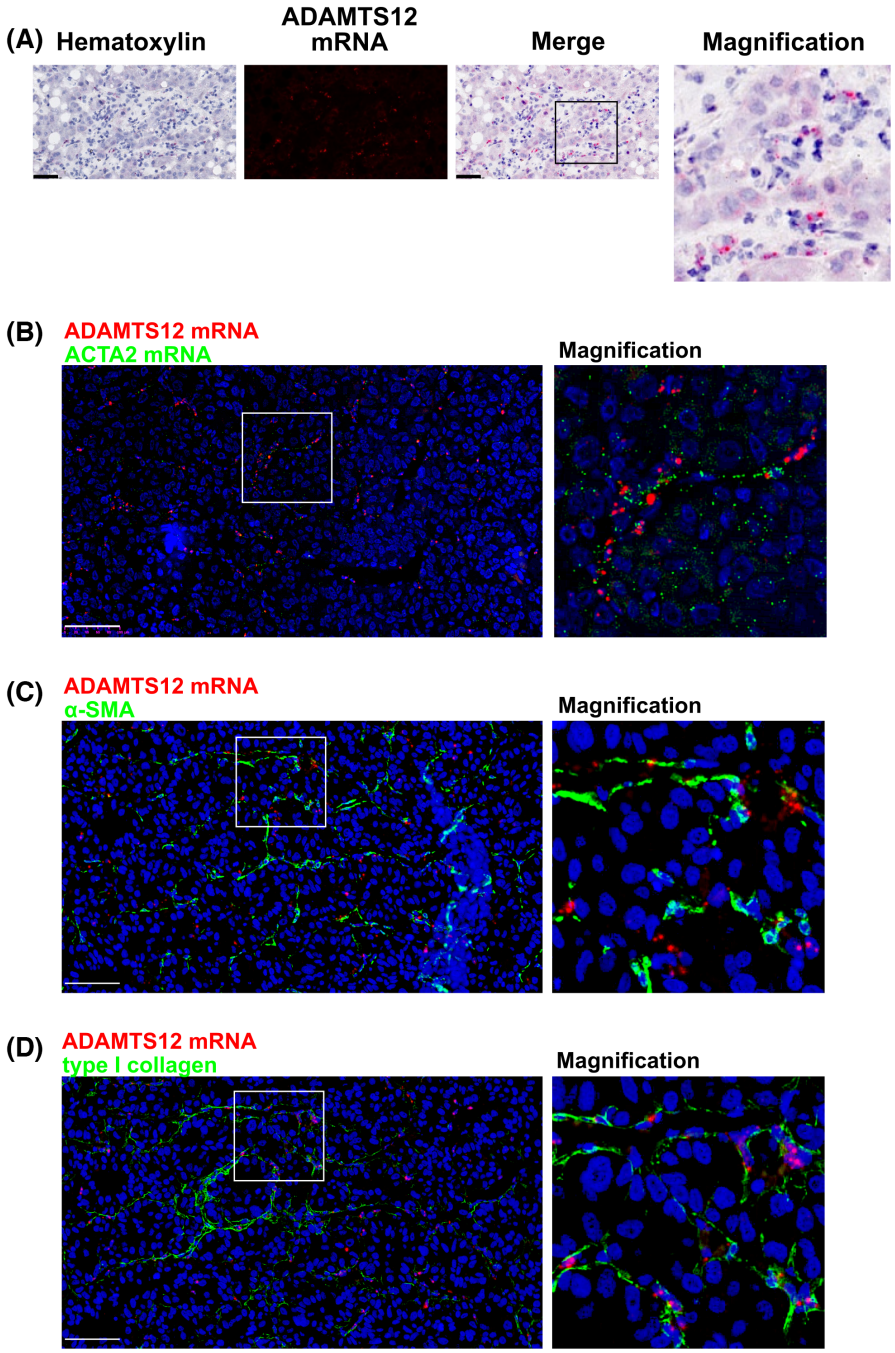

FIGURE 3 Stromal cells are the main sources of *ADAMTS12* expression in HCC. *ADAMTS12* expression was investigated in tumorss. (A) Histological sections counterstained with Hematoxylin. *ADAMTS12* transcripts were detected by in-situ hybridization (ISH) with specific probes and revealed by Fast-Red reagent. ISH signal was detected either under visible light together with Hematoxylin staining (left picture) or by epifluorescence at 550 nm (second picture from the left). Merged pictures are shown on the right. Red dots correspond to labeled mRNA molecules. Bar scales correspond to 50 µm. Regions selected for magnification are indicated by a square. (B) *ADAMTS12* (red labeling) and *ACTA2* (green labeling) transcripts co-detected by ISH in tumors. (C, D) *ADAMTS12* mRNA detected by ISH (red labeling) together with α-SMA (C) and type-1 collagen (D) immuno-labeled proteins (green labeling). Nuclei are counter-stained with Hoechst-33342. Bar scales for B–D: 100 µm Regions selected for magnification are indicated by a square.

observations, *ADAMTS12* expression in other HCC cell lines from the Cancer Cell Line Encyclopedia (CCLE) was very low compared with the expression of other adamalysins in these cells (Figure S6B). Overall, these observations indicate that *ADAMTS12* is expressed in stromal cells including activated HSCs and a limited number of endothelial cells. In non-tumor fibrotic tissues, these cells are in close proximity to immune infiltrates but distinct from monocytes and macrophages. Consistent with these observations, *ADAMTS12* expression is associated with signatures related to stromal activity, such as "leukocyte estimate" and "intratumoral fibrosis" in HCC samples (Table S3). In addition, these expression patterns are also in line with single-cell RNAseq data[31] showing that in the liver, *ADAMTS12* expression is restricted to HSCs and a limited number of endothelial cells (Figure S7).

3.5 | Fibrosis is exacerbated in *Adamts12*-null mice

Because activated HSCs play a central role in the response to liver injury, we explored the impact of *ADAMTS12* expression at the tissue level in a model of liver injury induced by CCl_4 treatment. We first explored the dynamics of *Adamts12* expression in response to acute liver injury

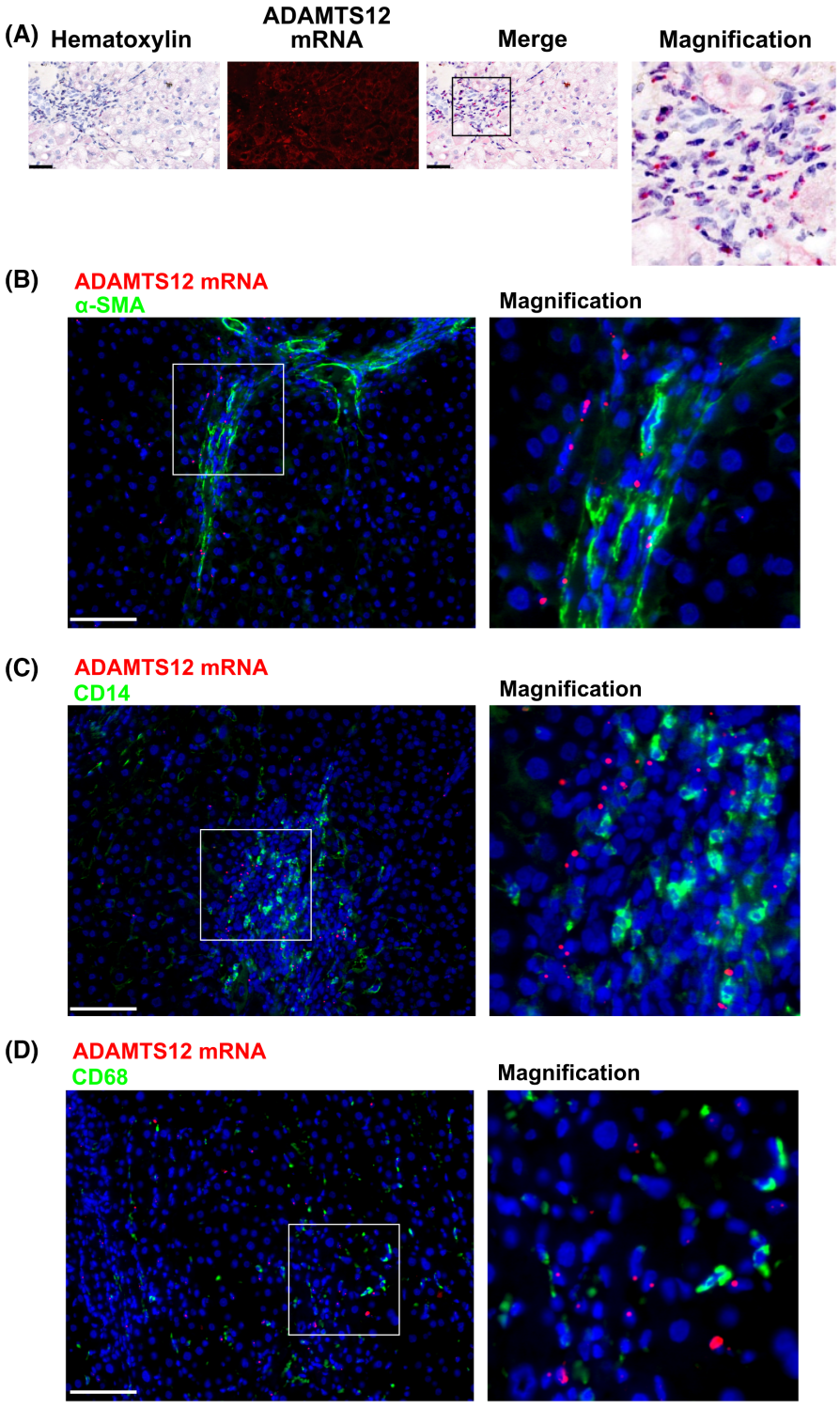

FIGURE 4 Stromal cells are the main sources of *ADAMTS12* expression in tumor-adjacent tissues. *ADAMTS12* expression was investigated in tumor-adjacent tissues shown in Figure 3. (A) *ADAMTS12* transcripts detected by in-situ hybridization (ISH) with specific probes and revealed by Fast-Red reagent. Histological sections were counterstained with Hematoxylin. The ISH signal was detected either under visible light together with Hematoxylin staining (left picture) or by epifluorescence at 550 nm (second picture from the left). Merged pictures are shown on the right. Red dots correspond to labeled mRNA molecules. Bar scales correspond to 50 μm. Regions selected for magnification are indicated by a square. (B–D) *ADAMTS12* mRNA detected by ISH (red labeling) together with α-SMA (B), CD14 (C) and CD68 (D) proteins (green labeling). Nuclei were counterstained with Hoechst-33342. Bar scales for B, C: 100 μm. Regions selected for magnification are indicated by a square.

in mice treated with a single injection of CCl_4. As shown in Figure 5, *Adamts12* mRNA levels were increased in the liver 24 h after CCl_4 injection compared with control mice injected with vehicle. This transient increase in *Adamts12* expression was concomitant with hepatolysis, monitored by plasma ALT activity (Figure S8C), and with the inflammatory response, illustrated by up-regulation of the inflammation marker genes IL1-β (*Il1b*), TNF-α (*Tnfa*), and *Inos* in the liver at 12 and 24 h (Figure 5B–D). After 7 days, the expression of *Adamts12* and inflammatory markers returned to levels similar to those in control mice. In a chronic injury model in which animals were repeatedly treated with CCl_4 (3 injections per week for 4 weeks), expression levels of *Adamts12* (measured 4 days after the last injection) remained unchanged compared with vehicle-treated control mice, as did expression levels of the inflammation marker TNF-α (Figure S9). The induction of *Adamts12* expression was therefore limited to the acute

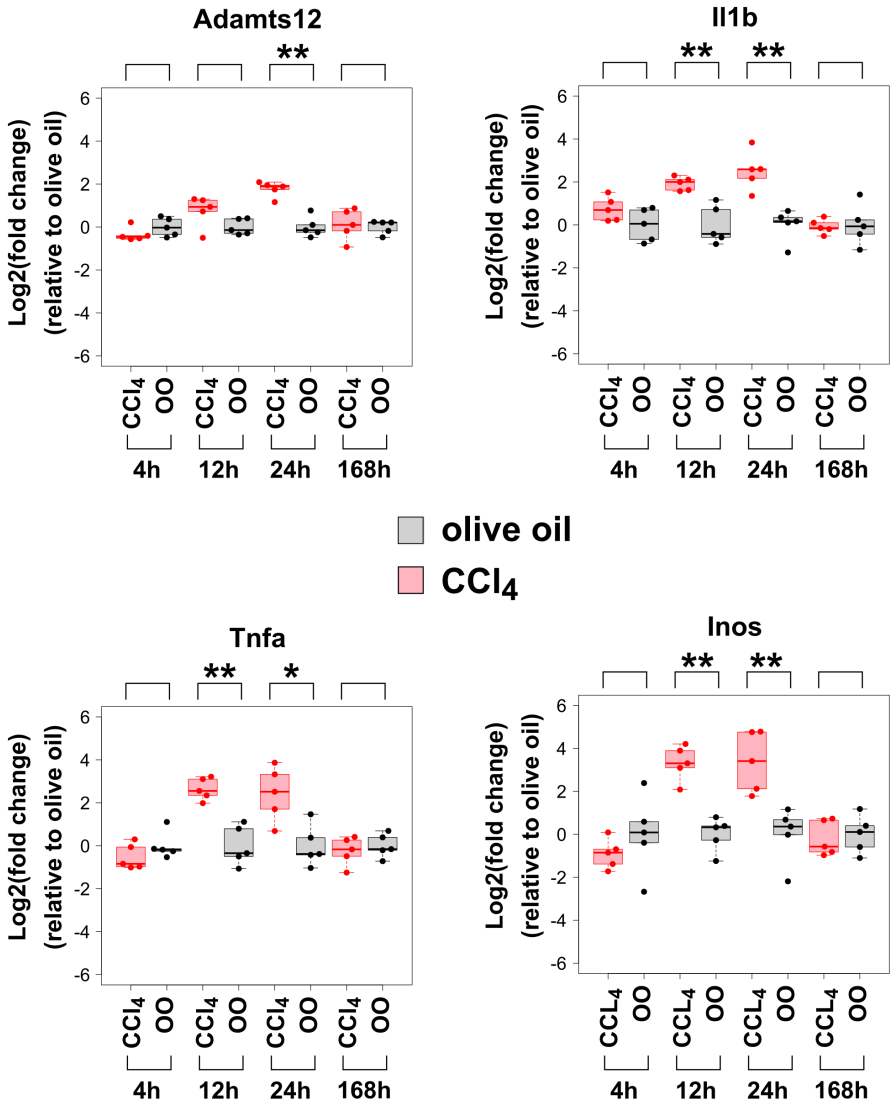

FIGURE 5 Expression of *Adamts12* and immune response markers at early stages of liver injury in livers from wild-type and *Adamts12*$^{-/-}$ mice. C57BL/6J mice received a single dose of 0.3 mL/Kg of CCl_4 by peritoneal injection and were sacrificed at 4, 12, 24 and 168 h (7 days) post injection. Gene expression levels in the liver were measured by RT-qPCR. Expression values of indicated genes in CCl_4 samples (red/pink) relative to control mice treated with vehicle (olive oil, OO, black/gray) are represented as fold changes in Log2. For each condition, dots represent expression values from five individuals. Note that Il1b gene expression data were previously reported in Ref. [32].

phase of the liver injury. Neither hepatolysis (ALT activity) nor the expression of the inflammation marker TNF-α was affected in *Adamts12*-null mice in response to acute injury, compared with the wild type (Figure S8). To assess whether *Adamts12* invalidation may impact tissue repair during chronic injury, fibrillar collagen deposition in the liver was analyzed by Sirius Red staining. As expected, we observed an increase in collagen deposition in mice repeatedly treated with CCl_4 compared with control mice treated with vehicle (Figure 6A, top picture). Importantly, this deposition was significantly greater in *Adamts12*$^{-/-}$ mice than in wild-type mice (Figure 6A, bottom picture, 6B, and Figure S10), indicating that fibrosis is exacerbated in *Adamts12*-null mice. Of note, the level of expression of Col1a1 in response to CCl_4 treatment was not significantly different in wild-type and *Adamts12*$^{-/-}$ mice, although the induction of Col1a1 expression in response to CCL4 was more marked in *Adamts12*$^{-/-}$ mice (Figure 6C). These observations indicate that tissue repair is altered in the absence of ADAMTS12.

3.6 | *Adamts12* invalidation affects the global response to liver injury

Since *Adamts12* expression is transiently induced upon acute injury, we characterized the global effects of *Adamts12* invalidation on the liver response. To this end we analyzed transcriptome dynamics in liver samples from both wild-type and *Adamts12*$^{-/-}$ mice at different time points after injury (GEO dataset: GSE224052). As expected, RNAseq data showed that in wild-type mice, CCl_4 treatment induces profound changes in gene expression (Table S4). Genes down-regulated at 4, 12 and 24 h after injury were enriched in ontologies related to metabolic pathways, whereas genes up-regulated at 4 and 12 h were related to gene expression machinery and cellular response to stress. Genes up-regulated at 24 h were enriched in ontologies related to leukocyte migration and chemotaxis. At 7 days, down-regulated genes were enriched in ontologies related to the cell division machinery, whereas up-regulated genes were related to

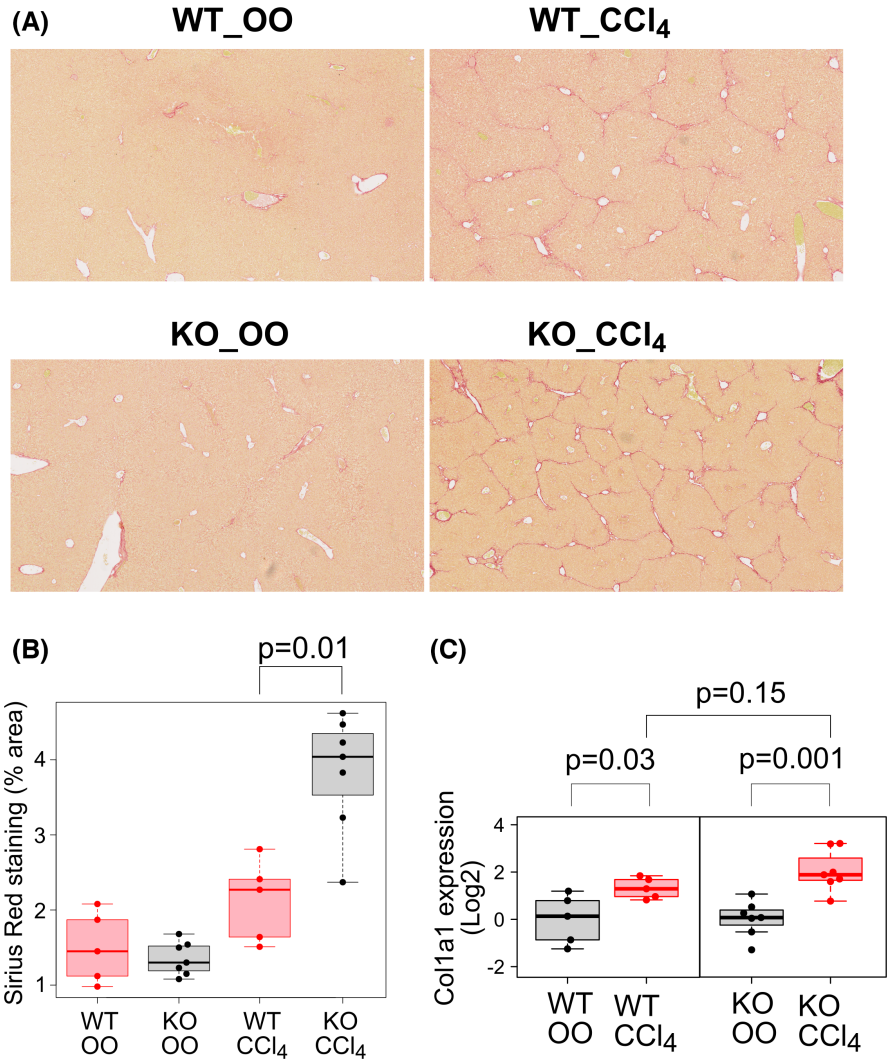

FIGURE 6 Fibrosis is exacerbated in *Adamts12*-null mice. Collagen deposit and expression were analyzed in chronic CCl_4–induced liver fibrosis mouse models. Mice received an intraperitoneal injection of CCl_4 (0.3 mL/Kg) three times per week for four weeks and were sacrificed 4 days after the last CCl_4 injection. (A) Liver sections from WT and *Adamts12*$^{-/-}$ (KO) mice treated with CCl_4 or vehicle (olive oil, OO) stained with Sirius red. (B) Quantification of fibrosis areas performed as described in experimental procedure and in Figure S10. Results are expressed as average percentage of the field tissue area. (C) Col1a1 gene expression measured by RT-qPCR in samples from WT and *Adamts12*$^{-/-}$ (KO) mice treated with CCl_4 or olive oil (OO) as indicated.

cytoplasmic translation and metabolism. These dynamics were essentially similar in *Adamts12*-invalidated mice, albeit with a smaller amplitude, specifically at 12 h and 7 days (Table S4). This indicates that some aspects of the liver response to injury are impacted by *Adamts12* invalidation. Consistent with this, genes up-regulated at 4 and 12 h after CCl_4 treatment in *Adamts12*$^{-/-}$ mice were enriched in ontologies related to the activation of immune response compared to wild-type mice (Table S5). When examining the up-regulated genes belonging to these ontologies, we found that several of them are markers of macrophages, monocytes and granulocytes (Figure S11). Interestingly, genes down-regulated in *Adamts12*$^{-/-}$ mice (with respect to wild-type) after 24 h of CCl_4 treatment were enriched in ontologies related to the adaptative immune response, and more specifically to the activation of T cells. We found that several of these genes are markers of both T and innate lymphocytes, including natural killers (NK) (Figure S12). Altogether, these expression data show global effects of *Adamts12* invalidation on the dynamic of the immune response to liver injury.

3.7 | Gene expression is profoundly affected by *ADAMTS12* silencing in HSC-derived LX-2 cells

Activated HSCs are stromal cells that play an important role in tissue repair and fibrosis through remodeling of the microenvironment. Since *ADAMTS12* is expressed in HSCs, some of the observed effects of *ADAMTS12* invalidation on tissue repair can arise from alterations of these cells. We therefore analyzed the effects of silencing *ADAMTS12* expression by RNA interference on the characteristics of the HSC-derived LX-2 cell line.[33] We first analyzed the transcriptomic changes induced by *ADAMTS12* silencing in these cells by RNA-seq analysis. As shown in the differential expression analysis (Table S6), *ADAMTS12* expression was silenced by

more than 70% after 48 h of siRNA treatment. Global transcriptome analysis showed that *ADAMTS12* knockdown resulted in profound changes in gene expression with 4662 differentially expressed genes (FDR < 0.05) of which 1992 were upregulated and 2670 downregulated (Figure 7A). Genes that were upregulated in *ADAMTS12*-deficient LX-2 cells were enriched in gene ontologies related to primary cilium and Smoothened (SMO) signaling pathway (Figure 7C). In line with these changes, we observed that the proportion of ciliated cells, as monitored with cilium axoneme marker (ARL13B),[34] was significantly increased in *ADAMTS12*-deprived cells compared with control cells (Figure S13). Of note, this increase in ciliated cells was mainly made up of cells with short cilia.

3.8 | *ADAMTS12* silencing impacts expression of genes involved in ECM remodeling

Down-regulated genes were enriched in gene ontologies related to extracellular structure organization, cell adhesion, cell migration, leukocyte migration, chemotaxis and actin filament organization (Figure 7D). Among these ontologies, several have known functions in ECM remodeling, including *MMP9* and *SERPINE1*, encoding the fibrogenic protein PAI-1.

Consistent with previous reports,[35,36] we observed that both MMP-9 expression and activity were stimulated by IL1-β in LX-2 cells, and we showed that both were down-regulated in *ADAMTS12*-silenced cells, whereas MMP-2

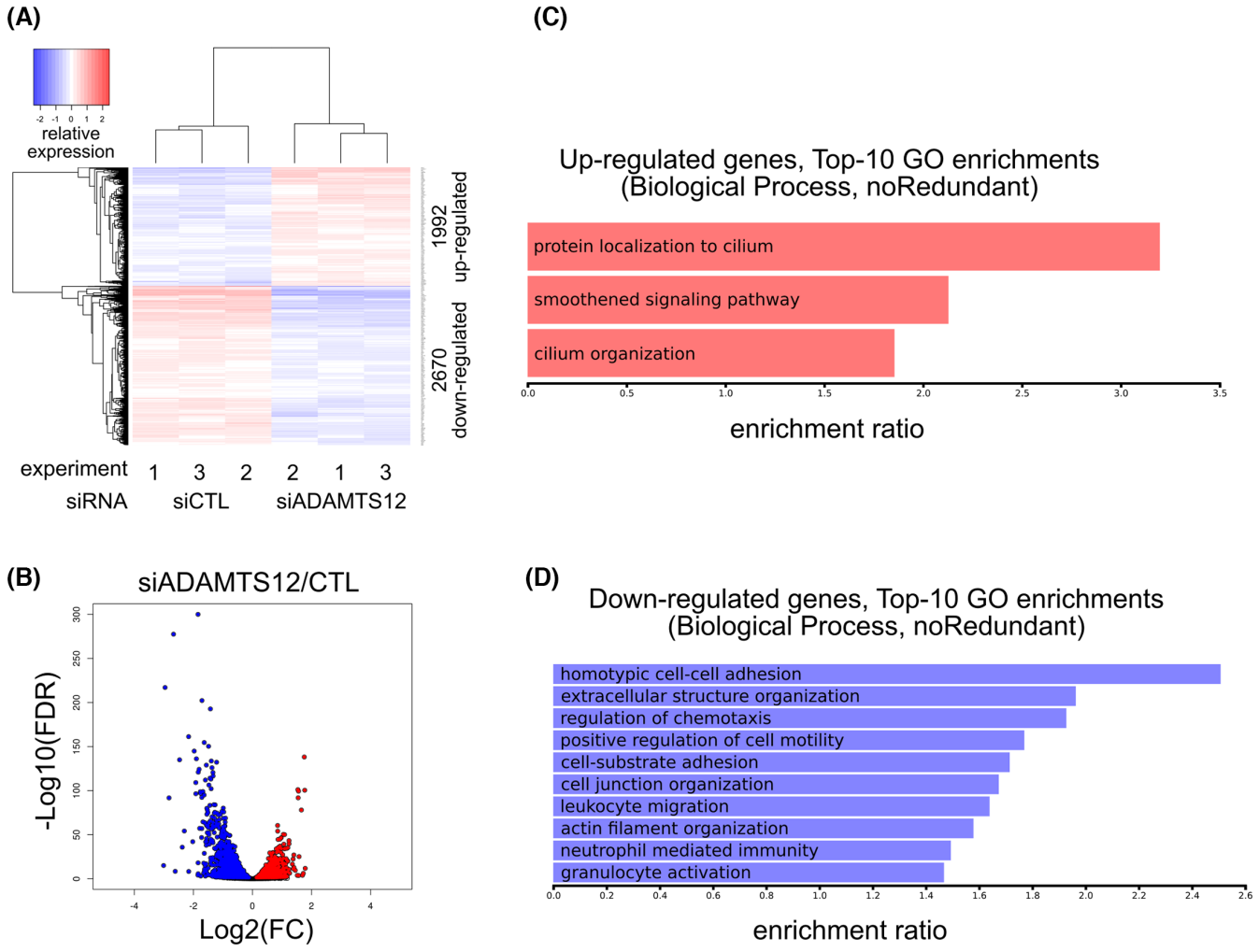

FIGURE 7 Differential expression of genes in *ADAMTS12*-silenced LX-2 cells. LX-2 cells were treated with a control siRNA (siCTL) or an siRNA against *ADAMTS12* mRNA (si*ADAMTS12*). RNA samples were collected 48 h after siRNA treatment and analyzed by RNA-sequencing. (A) Expression heat-map and clustering of 4662 differentially expressed genes (DEGs: FDR < 0.05) in three independent experiments. (B) Volcano plot showing differential expression of all genes. Down-regulated genes and up-regulated genes (FDR < 0.05) are colored in blue and red, respectively. (C, D) Enrichment of up-regulated genes (C) and down-regulated genes (D) in gene ontologies (GO Biological Process, non-redundant). Only enrichments with an FDR < 0.05 are represented. For down-regulated genes, only the top-ten enrichments are represented.

expression and activity remained constant (Figure S14). As shown in Figure S15, *SERPINE1* expression was induced by TGF-β treatment, in line with previous observations.[37] Interestingly, *SERPINE1* expression was down-regulated upon *ADAMTS12* silencing, in both TGF-β treated and untreated cells. In *ADAMTS12*-silenced cells, *SERPINE1* expression remained inducible by TGF-β (with similar induction rates as in control cells), although TGF-β treatment had no significant effect on *ADAMTS12* expression. This indicates that *ADAMTS12* silencing impacts *SERPINE1* expression, but not the response to TGF-β per se. Importantly, these combined effects of *ADAMTS12* expression and TGF-β on *SERPINE1* expression were similarly observed in primary activated HSCs (Figure S16) and fetal lung fibroblasts (MRC-5 cell line) (Figure S17).

These observations indicate that *ADAMTS12* expression in HSCs may impact ECM remodeling.

3.9 | The nuclear shape is altered in *ADAMTS12*-silenced LX-2 cells

ACTR3, encoding the Arp3 subunit of the Arp2/3 complex (involved in Actin assembly), is one of the more strongly down-regulated genes in *ADAMTS12*-silenced LX-2 cells (Table S6). At the cellular level, we observed a disorganization of actin filaments upon *ADAMTS12* silencing (Figure 8A). Because actin stress fibers provide a mechanical link between the cell surface and the nucleus,[38,39] we used nuclear shape as a readout of mechanical tensions exerted on the nuclei.[40] We observed that the projected areas of the nuclei were increased upon TGF-β treatment, and markedly reduced after *ADAMTS12* knockdown, in both untreated and TGF-β treated cells (Figure 8B,C), consistent with a decrease in tensions exerted by the cytoskeleton. Total DNA content, as measured by integrated Hoechst staining, was not affected (Figure S18), indicating that these changes in projected areas actually reflected changes in nuclear shape. Importantly, nuclear area was increased by TGF-β in both control and silenced cells (Figure 8B), confirming that, as for *SERPINE1* induction, response to TGF-β per se was not affected by *ADAMTS12* knock-down in LX-2 cells. These effects of TGF-β on nuclear size were similarly observed in primary cultures of HSCs and in MRC-5 fibroblasts while *ADAMTS12* silencing had no significant effect (Figure S19).

3.10 | The gene expression program of *ADAMTS12*-Silenced LX-2 cells shows an intermediate state of differentiation

The aforementioned phenotype changes observed in *ADAMTS12*-silenced LX-2 cells are suggestive of a less differentiated state with respect to the myofibroblastic phenotype which is characterized by cytoskeletal contractility and the production of ECM proteins. Of note, the *ADAMTS12* gene was identified as being up-regulated upon HSC activation both in vivo[41] and in vitro.[42,43]

To better characterize the phenotype of *ADAMTS12*-silenced LX-2, we analyzed the expression of gene signatures previously associated with different states of HSCs (Figure S20). Human orthologs of the 623 genes induced upon HSC activation in vivo[41] were predominantly down-regulated in LX-2 cells lacking ADAMTS12 (Figure S20A). However, some of these genes were not impacted (such as ACTA2 and TGFB2) or even up-regulated (such as INAVA and CCNE1). Similarly, gene sets whose expression is specific to different populations of activated HSCs in a model of Non-Alcoholic Steato-Hepatitis (NASH) fibrosis[44] were mostly down-regulated in *ADAMTS12*-silenced LX-2 cells, although some of them were not impacted or up-regulated (Figure S20B,C). Interestingly gene signatures of both quiescent or inactivated HSCs (Figure S20D,E) were also mostly down-regulated in LX-2 cells after *ADAMTS12* silencing.

Finally, genes previously characterized as being either up- or down-regulated upon in vitro activation of HSCs[42,43] were found mostly down-regulated in LX-2 cells following *ADAMTS12* knock-down (Figure S20G–J), and the same was true for genes either up- or down-regulated upon HSC reversion in vitro[45] (Figure S20K,L).

Altogether, these observations indicate that *ADAMTS12* knockdown leads to a global down-regulation of genes expressed in activated HSCs, but does not recapitulate a canonical inactivation program.

4 | DISCUSSION

Adamalysins are important players of the cellular microenvironment and several of them have been involved in tumor progression. In this study, we aimed at finding new members of this family that might play a role in the progression of the chronic liver disease including fibrosis and hepatocellular carcinoma (HCC). We found a cluster of seven ADAMTS and ADAMTSL proteins whose expression levels are strongly correlated in HCC. Among these proteins, ADAMTS12 was the one whose expression was most strongly associated with molecular signatures related to HCC progression and aggressiveness.

Previous publications have addressed the role of ADAMTS12 in various cancer types, with either pro- or anti-tumor roles. In lung cancer, truncating mutations have been associated with poor survival[46] while stromal expression of *ADAMTS12* was associated with better survival in colorectal cancer.[47] Conversely, expression of

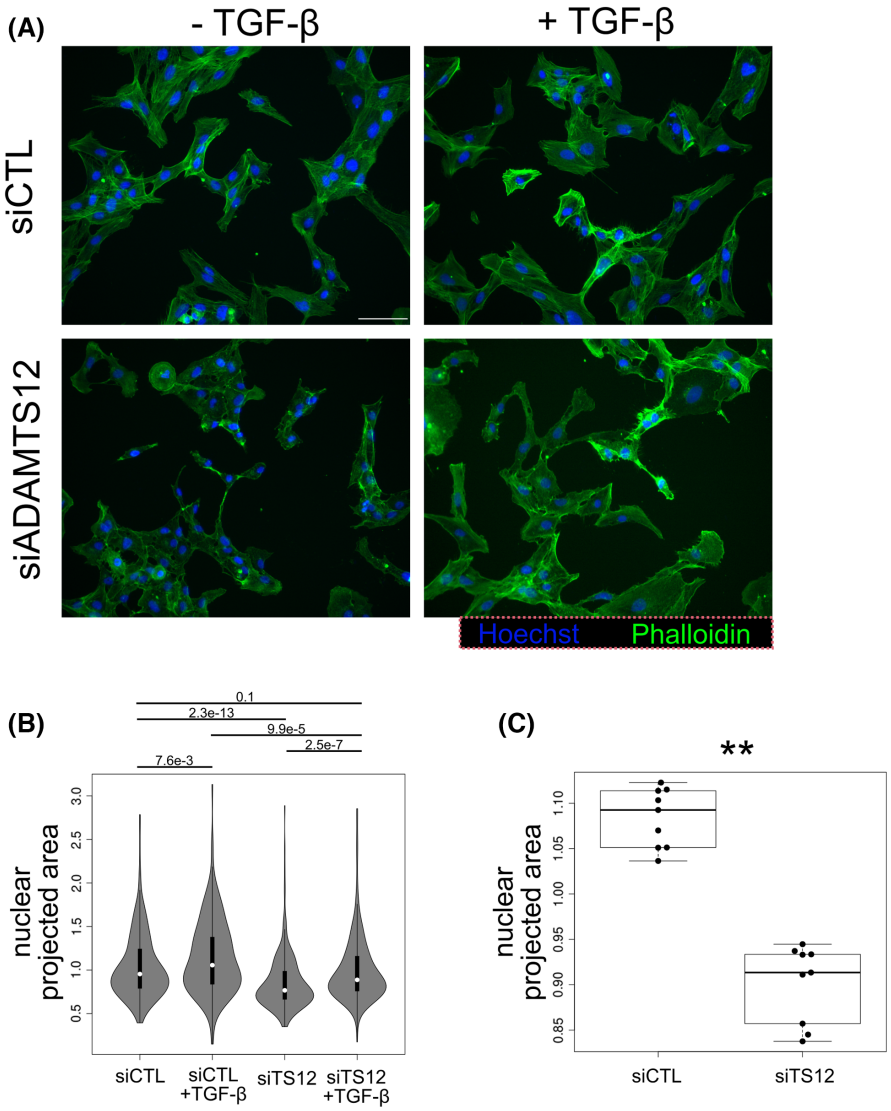

FIGURE 8 Mechanical tension exerted on nuclei is reduced in *ADAMTS12*-silenced LX-2 cells. (A) Cells treated for 48 h with control (siCTL) or *ADAMTS12* (si*ADAMTS12*) siRNAs, and cultured for an additional 24 h in the presence or absence of TGF-β as indicated. Cells were fixed and F-Actin (green) was detected by incubation with phalloidin-AlexaFluor-488. Nuclei where counter-stained with Hoechst-33342. Scale bar: 100 μm. (B) Projected areas of nuclei measured and plotted as violin plots. 317, 182, 271 and 234 nuclei were measured for the groups siCTL, siCTL + TGF-β, siTS12 (si*ADAMTS12*) and siTS12 + TGF-β, respectively. Adjusted *p*-values of a Kruskal–Wallis multiple comparison test are indicated. (C) Average projected areas of Hoechst-stained nuclei from 9 independent experiments comparing cells treated with siCTL and si*ADAMTS12* siRNAs. Paired *t*-test comparisons (**$p < .01$).

ADAMTS12 in pancreatic cancer cells promotes EMT and therefore potentially invasion[48] while high expression of *ADAMTS12* in gastric cancer is associated with poor prognosis, and a signature of Treg infiltration.[49]

In the liver, single-nucleotide variations in the *ADAMTS12* gene were found in cell-free DNA of 5 patients with HCC out of 30, and in tumor samples of 15 patients out of 366,[50] although no functional link between these variants and HCC progression has been established.

To our knowledge, the present study is the first characterization of ADAMTS12 in chronic liver disease (CLD).

In the case of HCC, we demonstrated that *ADAMTS12* is expressed in both tumor and non-tumor tissues, and its expression is restricted to stromal cells, particularly activated hepatic stellate cells (aHSCs). aHSCs are considered as liver mesenchymal stem cells (MSCs)[51] and play important roles in chronic liver disease (CLD) progression, including fibrosis (reviewed in Ref. [5]) and HCC.[52,53] While *ADAMTS12* expression in tumor-associated MSCs has been previously observed in a model of primary lung cancer,[54] to our knowledge its expression in HCC stromal cells has not been described so far. Previous studies have shown that *ADAMTS12* expression is induced upon HSC activation in vitro (from isolated quiescent HSC) and in vivo (in animal models of fibrosis).[41–43] Consistent with these observations, we showed that *ADAMTS12* expression is transiently induced after acute liver injury, along with hepatolysis and inflammation markers. Chronic injury leads to collagen accumulation and fibrosis, and we found that fibrosis was markedly exacerbated in *Adamts12*-invalidated mice, indicating that the response to injury is altered in these mice.

To evaluate the contribution of HSCs in the effects of *Adamts12* invalidation seen in mice, we used the HSC-derived cell line LX-2[33] as a model to investigate the possible roles of ADAMTS12 in controlling HSC phenotype. Among other ADAMTS family members, *ADAMTS12* is the gene with the highest expression level in these cells (GEO dataset: GSE223753). We demonstrated that

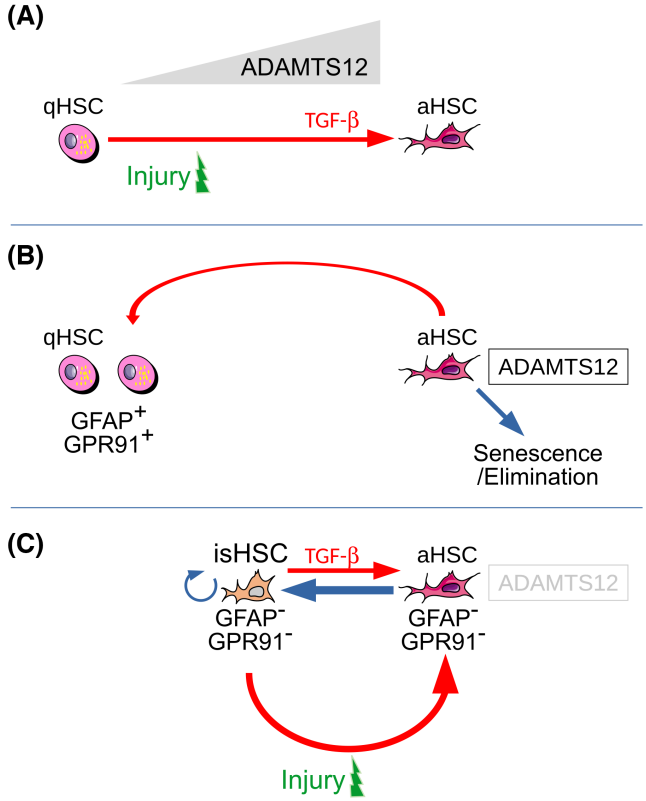

FIGURE 9 Hypothetic scheme for ADAMTS12 action in hepatic stellate cells (HSCs). (A) Upon liver injury, quiescent HSCs (qHSCs) transform into myofibroblastic activated HSCs (aHSCs) which participate in tissue repair. HSC activation involves inflammatory signals and TGF-β. Together with fibrogenic genes, *ADAMTS12* expression is induced during this process. (B) At the end of injury, a subpopulation of aHSCs enters senescence and is eliminated by the immune system, while another subpopulation reverts towards a phenotype (GFAP- and GPR91-positive) close to the quiescent state. (C) In the absence of ADAMTS12, the fate of activated HSCs is skewed towards a self-renewable and reactivatable "intermediate state" (isHSCs) which in turn promote fibrosis upon repeated injuries. Although possibly different from the previously characterized inactivated state (iHSCs),[44,63] these isHSCs constitute a stock of self-renewing mesenchymal cells which escape elimination and can be reactivated by TGF-β and upon successive repeated injuries.

inhibition of *ADAMTS12* expression resulted in profound changes in the gene expression program of LX-2 cells. Genes up-regulated after *ADAMTS12* knockdown were related to the smoothened (SMO) signaling pathway. SMO is an effector of Hedgehog (Hh) signaling. While a limited number of activated HSCs express a primary cilium, the observed increase in cells with short cilia upon *ADAMTS12* silencing may in turn modulate SMO/hedgehog signaling which requires translocation of SMO to cilia.[55] In the context of liver injury, Hh signaling was shown to regulate both tissue regeneration and fibrosis by controlling the fate of HSCs.[56] Modulating this pathway in HSCs might therefore contribute to impairing the balance between liver repair and fibrosis.

Genes downregulated upon *ADAMTS12* knockdown were enriched in ontologies related to extracellular structure and actin filament organization. Accordingly, we showed that actin fiber organization was altered in these cells. Stress fibers establish a physical link between the plasma membrane and the nuclear envelope and exert mechanical constraints on the shape of the nucleus.[38–40] Consistent with a weakening of these constraints, nuclei appeared less spread, as evidenced by significantly smaller projected areas.

Cell mechanical properties and cilium biogenesis are intimately dependent on F-Actin dynamics. Strikingly, the most strongly downregulated gene in *ADAMTS12*-silenced LX-2 cells is ACTR3, encoding the Arp3 subunit of the Arp2/3 complex (Table S6) whose role in actin polymerization has been extensively documented. A partial loss of ACTR3 function could therefore be sufficient to induce changes in both mechanical stress and primary cilium functions.[57,58] However, the observed phenotypic changes probably result from a more global effect of ADAMTS12 depletion as seen by the global decrease of HSC activation markers. Because ADAMTS12 is intimately bound to the cell surface,[59] this protein may be involved in subtle ECM remodeling in close vicinity to the cell. By altering the mechanical tension exerted on the nucleus, these changes would in turn affect the overall expression program,[40] thereby modulating the phenotype of HSCs towards a less differentiated state, in line with previous studies showing that HSC activation is promoted by both TGF-β signaling and ECM stiffness.[60] Reciprocally, these mechanical effects of *ADAMTS12* silencing on the nuclear shape were observed in LX-2 cells which exhibit a partially activated phenotype[61] but not in fully activated primary HSCs, indicating that these effects are restrained to intermediate differentiation states. TGF-β treatment increased the mechanical tension exerted on nuclei without restoring *ADAMTS12* expression (Figure S15). Importantly, the TGF-β response per se, as monitored by *SERPINE1* induction, was not affected by ADAMTS12 depletion. Of note, *SERPINE1* expression is induced by both TGF-β and ECM stiffness mechanotransduction.[62] In the context of repetitive liver injuries, we propose that the effects of *Adamts12* knockout on the mechanical properties of HSCs could be overcome by the TGF-β signal produced upon each injury, while promoting an intermediate state (isHSC) in periods of recovery, when TGF-β levels are decreased. Using GFAP[63] and GPR91[64] as markers of quiescent HSCs (qHSCs), we observed that GFAP- and GPR91-positive cell populations increase in the liver seven days after acute injury. This suggests that HSCs accumulate at the end of recovery, with a phenotype (GFAP- and GPR91-positive) close to the quiescent state.

Interestingly, this accumulation is not observed in mice invalidated for ADAMTS12 (Figure S21), indicating that HSC homeostasis is modulated by ADAMTS12. In the absence of ADAMTS12, HSCs might accumulate with a different phenotype (GFAP- and GPR91-negative), which could be more responsive to successive injuries. Although possibly different from the previously described inactivated state (iHSCs),[44,63] this intermediate state would maintain a reactivatable cell population that escapes elimination by apoptosis or senescence[65] (Figure 9). In line with this model, genes previously associated with replicative senescence are globally down-regulated after *ADAMTS12* silencing in LX-2 cells (Figure S22). Previous studies have shown that ADAMTS12 acts as a modulator of inflammation.[66,67] Here, we show that expression of genes related to the immune response is impaired in *Adamts12*-invalidated mice following acute liver injury. The exacerbated liver fibrosis in null mice could therefore be a consequence of deregulations that may impact the early inflammatory response and/or HSC clearance. The observed deregulation of genes related to extracellular remodeling, chemotaxis and leukocyte migration in *ADAMTS12*-silenced HSCs might contribute to these outcomes, although these cannot be inferred directly from the behavior of isolated cells.

Altogether, our data indicate that *ADAMTS12* is expressed by stromal cells including HSCs, and that it modulates the balance between tissue repair and fibrosis at both cell autonomous (by controlling HSC homeostasis) and non-autonomous levels.

AUTHOR CONTRIBUTIONS

Bassil Dekky, Christine Monseur, Fida Azar, Dominique Bonnier, Esther Arpigny, Chiara Kalebic and Vincent Legagneux performed the wet-lab experiments. Alain Colige supervised experimentations with in vivo models and their analyses. Nathalie Théret and Vincent Legagneux performed bioinformatics analyses. All authors read and approved the final manuscript.

ACKNOWLEDGMENTS

This work was supported by the Institut National de la Santé et de la Recherche Médicale (INSERM), Université de Rennes 1, the Ligue Contre le Cancer and the Région Bretagne. BD was recipient of PhD fellowships from the Ligue Contre le Cancer and Région Bretagne. A. C. and C. M are supported by the "Fonds de la Recherche Scientifique–FNRS" (Grant 7.6536.18), the "Fonds Léon Frédéricq" and ULiège. The authors thank the Rennes Biological Resources Center (CHRU Pontchaillou, IFR 140) for its contribution to human tissue sampling, and the Biosit H2P2 facility for histological studies. We acknowledge the excellent support of the GIGA center at University of Liege, Belgium, in which the animal experimentations were carried out. RNA-sequencing (libraries, runs and primary analyses) was performed by the GenoBiRD facility homed by the Structure Fédérative de Recherche en Santé François Bonamy, University of Nantes (France). Histopathological analyses were performed at the HistoPathology of High Precision facility (H2P2) hosted at UMS Biosit (Inserm UMS 018, CNRS UMS3480). Computing resources were provided by the GenOuest Bioinformatics, a BioGenOuest facility hosted at IRISA/INRIA Rennes Bretagne Atlantique. The authors thank Dr. C. Lucas (Service Biochimie, CHU Rennes) for enzyme measurements, Dr Vincent Guen (CNRS, University of Rennes, France) and Bruno Turlin (Univ Rennes, CHU Rennes, F-35000 Rennes, France) for fruitful discussions, Frederic Ezan and Michel Rauch for technical assistance, Olivier Collin for the excellent support of the GenOuest bioinformatics core facility, Servane Le Page and Laurence Huc for providing anti-GPR91 antibodies, and Dr Catherine Lavau (Inserm U1085, University of Rennes 1) for critical reading of the manuscript. Fida Azar's thesis was co-financed by the municipality of Hayata (Lebanon) and supervised within the frame of a partnership between le Lebanese University (Beirut, Lebanon) and the University of Rennes (France).

DISCLOSURES

The authors have no conflict of interest to declare.

DATA AVAILABILITY STATEMENT

The raw (fastq files) and processed (normalized counts) RNA-seq data supporting this study have been deposited in the Gene Expression Omnibus repository with the following accession numbers: Murine liver samples: GSE224052; LX-2 cell line: GSE223753. Public TCGA expression data are from https://portal.gdc.cancer.gov/projects/TCGA-LIHC. Clinical and molecular attributes of these TCGA samples are from https://ars.els-cdn.com/content/image/1-s2.0-S0092867417306396-mmc1.xlsx.

ORCID

Bassil Dekky https://orcid.org/0000-0002-4235-7505
Fida Azar https://orcid.org/0000-0001-5946-9426
Alain Colige https://orcid.org/0000-0003-0957-1355
Vincent Legagneux https://orcid.org/0000-0002-1417-6678
Nathalie Théret https://orcid.org/0000-0002-5857-7828

REFERENCES

1. Théret N, Musso O, Turlin B, et al. Increased extracellular matrix remodeling is associated with tumor progression in human hepatocellular carcinomas. *Hepatology*. 2001;34:82-88.
2. Cordero-Espinoza L, Huch M. The balancing act of the liver: tissue regeneration versus fibrosis. *J Clin Invest*. 2018;128:85-96.
3. Naba A, Clauser KR, Hoersch S, Liu H, Carr SA, Hynes RO. The matrisome: in silico definition and in vivo characterization

by proteomics of normal and tumor extracellular matrices. *Mol Cell Proteomics*. 2012;11:M111.014647.

4. Massey VL, Dolin CE, Poole LG, et al. The hepatic "matrisome" responds dynamically to injury: characterization of transitional changes to the extracellular matrix in mice. *Hepatology*. 2017;65:969-982.
5. Tsuchida T, Friedman SL. Mechanisms of hepatic stellate cell activation. *Nat Rev Gastroenterol Hepatol*. 2017;14:397-411.
6. Théret N, Bouezzedine F, Azar F, Diab-Assaf M, Legagneux V. ADAM and ADAMTS proteins, new players in the regulation of hepatocellular carcinoma microenvironment. *Cancers (Basel)*. 2021;13:1563.
7. Edwards DR, Handsley MM, Pennington CJ. The ADAM metalloproteinases. *Mol Aspects Med*. 2008;29:258-289.
8. Apte SS. A disintegrin-like and metalloprotease (reprolysin-type) with thrombospondin type 1 motif (ADAMTS) superfamily: functions and mechanisms. *J Biol Chem*. 2009;284:31493-31497.
9. Le Pabic H, Bonnier D, Wewer UM, et al. ADAM12 in human liver cancers: TGF-beta-regulated expression in stellate cells is associated with matrix remodeling. *Hepatology*. 2003;37:1056-1066.
10. Atfi A, Dumont E, Colland F, et al. The disintegrin and metalloproteinase ADAM12 contributes to TGF-beta signaling through interaction with the type II receptor. *J Cell Biol*. 2007;178:201-208.
11. Leyme A, Bourd-Boittin K, Bonnier D, Falconer A, Arlot-Bonnemains Y, Théret N. Identification of ILK as a new partner of the ADAM12 disintegrin and metalloprotease in cell adhesion and survival. *Mol Biol Cell*. 2012;23:3461-3472.
12. Mazzocca A, Coppari R, De Franco R, et al. A secreted form of ADAM9 promotes carcinoma invasion through tumor-stromal interactions. *Cancer Res*. 2005;65:4728-4738.
13. Schwettmann L, Wehmeier M, Jokovic D, et al. Hepatic expression of A disintegrin and metalloproteinase (ADAM) and ADAMs with thrombospondin motives (ADAM-TS) enzymes in patients with chronic liver diseases. *J Hepatol*. 2008;49:243-250.
14. Bourd-Boittin K, Basset L, Bonnier D, L'helgoualc'h A, Samson M, Théret N. CX3CL1/fractalkine shedding by human hepatic stellate cells: contribution to chronic inflammation in the liver. *J Cell Mol Med*. 2009;13:1526-1535.
15. Fujita T, Maesawa C, Oikawa K, Nitta H, Wakabayashi G, Masuda T. Interferon-gamma down-regulates expression of tumor necrosis factor-alpha converting enzyme/a disintegrin and metalloproteinase 17 in activated hepatic stellate cells of rats. *Int J Mol Med*. 2006;17:605-616.
16. Oikawa H, Maesawa C, Tatemichi Y, et al. A disintegrin and metalloproteinase 17 (ADAM17) mediates epidermal growth factor receptor transactivation by angiotensin II on hepatic stellate cells. *Life Sci*. 2014;97:137-144.
17. Xia Y, Chen R, Song Z, et al. Gene expression profiles during activation of cultured rat hepatic stellate cells by tumoral hepatocytes and fetal bovine serum. *J Cancer Res Clin Oncol*. 2010;136:309-321.
18. Mazzocca A, Giannelli G, Antonaci S. Involvement of ADAMs in tumorigenesis and progression of hepatocellular carcinoma: is it merely fortuitous or a real pathogenic link? *Biochim Biophys Acta*. 2010;1806:74-81.
19. Goto K, Arai J, Stephanou A, Kato N. Novel therapeutic features of disulfiram against hepatocellular carcinoma cells with inhibitory effects on a disintegrin and metalloproteinase 10. *Oncotarget*. 2018;9:18821-18831.
20. Diamantis I, Lüthi M, Hösli M, Reichen J. Cloning of the rat ADAMTS-1 gene and its down regulation in endothelial cells in cirrhotic rats. *Liver*. 2000;20:165-172.
21. Bourd-Boittin K, Bonnier D, Leyme A, et al. Protease profiling of liver fibrosis reveals the ADAM metallopeptidase with thrombospondin type 1 motif, 1 as a central activator of transforming growth factor beta. *Hepatology*. 2011;54:2173-2184.
22. Kesteloot F, Desmoulière A, Leclercq I, et al. ADAM metallopeptidase with thrombospondin type 1 motif 2 inactivation reduces the extent and stability of carbon tetrachloride-induced hepatic fibrosis in mice. *Hepatology*. 2007;46:1620-1631.
23. Bekhouche M, Leduc C, Dupont L, et al. Determination of the substrate repertoire of ADAMTS2, 3, and 14 significantly broadens their functions and identifies extracellular matrix organization and TGF-β signaling as primary targets. *FASEB J*. 2016;30:1741-1756.
24. Bauters D, Spincemaille P, Geys L, et al. ADAMTS5 deficiency protects against non-alcoholic steatohepatitis in obesity. *Liver Int*. 2016;36:1848-1859.
25. Pi L, Jorgensen M, Oh S-H, et al. A disintegrin and metalloprotease with thrombospondin type I motif 7: a new protease for connective tissue growth factor in hepatic progenitor/oval cell niche. *Am J Pathol*. 2015;185:1552-1563.
26. Uemura M, Fujimura Y, Ko S, Matsumoto M, Nakajima Y, Fukui H. Pivotal role of ADAMTS13 function in liver diseases. *Int J Hematol*. 2010;91:20-29.
27. El Hour M, Moncada-Pazos A, Blacher S, et al. Higher sensitivity of Adamts12-deficient mice to tumor growth and angiogenesis. *Oncogene*. 2010;29:3025-3032.
28. Cancer Genome Atlas Research Network. Comprehensive and integrative genomic characterization of hepatocellular carcinoma. *Cell*. 2017;169:1327-1341.e23.
29. Bekhouche M, Colige A. The procollagen N-proteinases ADAMTS2, 3 and 14 in pathophysiology. *Matrix Biol*. 2015;44–46:46-53.
30. Bukong TN, Maurice SB, Chahal B, Schaeffer DF, Winwood PJ. Versican: a novel modulator of hepatic fibrosis. *Lab Invest*. 2016;96:361-374.
31. Guilliams M, Bonnardel J, Haest B, et al. Spatial proteogenomics reveals distinct and evolutionarily conserved hepatic macrophage niches. *Cell*. 2022;185:379-396.e38.
32. Azar F, Courtet K, Dekky B, et al. Integration of miRNA-regulatory networks in hepatic stellate cells identifies TIMP3 as a key factor in chronic liver disease. *Liver Int*. 2020;40:2021-2033.
33. Xu L, Hui AY, Albanis E, et al. Human hepatic stellate cell lines, LX-1 and LX-2: new tools for analysis of hepatic fibrosis. *Gut*. 2005;54:142-151.
34. Cantagrel V, Silhavy JL, Bielas SL, et al. Mutations in the cilia gene ARL13B lead to the classical form of Joubert syndrome. *Am J Hum Genet*. 2008;83:170-179.
35. Takahara T, Zhang LP, Yata Y, et al. Modulation of matrix metalloproteinase-9 in hepatic stellate cells by three-dimensional type I collagen: its activation and signaling pathway. *Hepatol Res*. 2003;26:318-326.

36. Robert S, Gicquel T, Bodin A, Lagente V, Boichot E. Characterization of the MMP/TIMP imbalance and collagen production induced by IL-1β or TNF-α release from human hepatic stellate cells. *PLoS ONE*. 2016;11:e0153118.
37. Tahashi Y, Matsuzaki K, Date M, et al. Differential regulation of TGF-beta signal in hepatic stellate cells between acute and chronic rat liver injury. *Hepatology*. 2002;35:49-61.
38. Maniotis AJ, Chen CS, Ingber DE. Demonstration of mechanical connections between integrins, cytoskeletal filaments, and nucleoplasm that stabilize nuclear structure. *Proc Natl Acad Sci U S A*. 1997;94:849-854.
39. Wang N, Tytell JD, Ingber DE. Mechanotransduction at a distance: mechanically coupling the extracellular matrix with the nucleus. *Nat Rev Mol Cell Biol*. 2009;10:75-82.
40. Thomas CH, Collier JH, Sfeir CS, Healy KE. Engineering gene expression and protein synthesis by modulation of nuclear shape. *Proc Natl Acad Sci U S A*. 2002;99:1972-1977.
41. De Smet V, Eysackers N, Merens V, et al. Initiation of hepatic stellate cell activation extends into chronic liver disease. *Cell Death Dis*. 2021;12:1110.
42. De Minicis S, Seki E, Uchinami H, et al. Gene expression profiles during hepatic stellate cell activation in culture and in vivo. *Gastroenterology*. 2007;132:1937-1946.
43. El Taghdouini A, Sørensen AL, Reiner AH, et al. Genome-wide analysis of DNA methylation and gene expression patterns in purified, uncultured human liver cells and activated hepatic stellate cells. *Oncotarget*. 2015;6:26729-26745.
44. Rosenthal SB, Liu X, Ganguly S, et al. Heterogeneity of HSCs in a mouse model of NASH. *Hepatology*. 2021;74:667-685.
45. El Taghdouini A, Najimi M, Sancho-Bru P, Sokal E, van Grunsven LA. In vitro reversion of activated primary human hepatic stellate cells. *Fibrogenesis Tissue Repair*. 2015;8:14.
46. Rabadán R, Mohamedi Y, Rubin U, et al. Identification of relevant genetic alterations in cancer using topological data analysis. *Nat Commun*. 2020;11:3808.
47. Wang D, Zhu T, Zhang F-B, He C. Expression of ADAMTS12 in colorectal cancer-associated stroma prevents cancer development and is a good prognostic indicator of colorectal cancer. *Dig Dis Sci*. 2011;56:3281-3287.
48. He R-Z, Zheng J-H, Yao H-F, et al. ADAMTS12 promotes migration and epithelial-mesenchymal transition and predicts poor prognosis for pancreatic cancer. *Hepatobiliary Pancreat Dis Int*. 2023;22(2):169-178.
49. Hu G, Sun N, Jiang J, Chen X. Establishment of a 5-gene risk model related to regulatory T cells for predicting gastric cancer prognosis. *Cancer Cell Int*. 2020;20:433.
50. Kunadirek P, Chuaypen N, Jenjaroenpun P, et al. Cell-free DNA analysis by whole-exome sequencing for hepatocellular carcinoma: a pilot study in Thailand. *Cancers (Basel)*. 2021;13:2229.
51. Kordes C, Sawitza I, Götze S, Häussinger D. Hepatic stellate cells support hematopoiesis and are liver-resident mesenchymal stem cells. *Cell Physiol Biochem*. 2013;31:290-304.
52. Amann T, Bataille F, Spruss T, et al. Activated hepatic stellate cells promote tumorigenicity of hepatocellular carcinoma. *Cancer Sci*. 2009;100:646-653.
53. Carloni V, Luong TV, Rombouts K. Hepatic stellate cells and extracellular matrix in hepatocellular carcinoma: more complicated than ever. *Liver Int*. 2014;34:834-843.
54. Fregni G, Quinodoz M, Möller E, et al. Reciprocal modulation of mesenchymal stem cells and tumor cells promotes lung cancer metastasis. *EBioMedicine*. 2018;29:128-145.
55. Corbit KC, Aanstad P, Singla V, Norman AR, Stainier DYR, Reiter JF. Vertebrate smoothened functions at the primary cilium. *Nature*. 2005;437:1018-1021.
56. Michelotti GA, Xie G, Swiderska M, et al. Smoothened is a master regulator of adult liver repair. *J Clin Invest*. 2013;123:2380-2394.
57. Pitaval A, Tseng Q, Bornens M, Théry M. Cell shape and contractility regulate ciliogenesis in cell cycle-arrested cells. *J Cell Biol*. 2010;191:303-312.
58. Drummond ML, Li M, Tarapore E, et al. Actin polymerization controls cilia-mediated signaling. *J Cell Biol*. 2018;217:3255-3266.
59. Bai XH, Wang DW, Luan Y, Yu XP, Liu CJ. Regulation of chondrocyte differentiation by ADAMTS-12 metalloproteinase depends on its enzymatic activity. *Cell Mol Life Sci*. 2009;66:667-680.
60. Olsen AL, Bloomer SA, Chan EP, et al. Hepatic stellate cells require a stiff environment for myofibroblastic differentiation. *Am J Physiol Gastrointest Liver Physiol*. 2011;301:G110-G118.
61. Weiskirchen R, Weimer J, Meurer SK, et al. Genetic characteristics of the human hepatic stellate cell line LX-2. *PLoS One*. 2013;8:e75692.
62. Dou C, Liu Z, Tu K, et al. P300 acetyltransferase mediates stiffness-induced activation of hepatic stellate cells into tumor-promoting myofibroblasts. *Gastroenterology*. 2018;154:2209-2221.e14.
63. Kisseleva T, Cong M, Paik Y, et al. Myofibroblasts revert to an inactive phenotype during regression of liver fibrosis. *Proc Natl Acad Sci U S A*. 2012;109:9448-9453.
64. Correa PRAV, Kruglov EA, Thompson M, Leite MF, Dranoff JA, Nathanson MH. Succinate is a paracrine signal for liver damage. *J Hepatol*. 2007;47:262-269.
65. Krizhanovsky V, Yon M, Dickins RA, et al. Senescence of activated stellate cells limits liver fibrosis. *Cell*. 2008;134:657-667.
66. Paulissen G, El Hour M, Rocks N, et al. Control of allergen-induced inflammation and hyperresponsiveness by the metalloproteinase ADAMTS-12. *J Immunol*. 2012;189:4135-4143.
67. Moncada-Pazos A, Obaya AJ, Llamazares M, et al. ADAMTS-12 metalloprotease is necessary for normal inflammatory response. *J Biol Chem*. 2012;287:39554-39563.

SUPPORTING INFORMATION

Additional supporting information can be found online in the Supporting Information section at the end of this article.

How to cite this article: Dekky B, Azar F, Bonnier D, et al. ADAMTS12 is a stromal modulator in chronic liver disease. *The FASEB Journal*. 2023;37:e23237. doi:10.1096/fj.202200692RRRR